Optics Communications 284 (2011) 3954–3964

Contents lists available at ScienceDirect

Optics Communications

journal homepage: www.elsevier.com/locate/optcom

Image hiding based on near-optimal moiré gratings

Edita Sakyte, Rita Palivonaite, Algiment Aleksa, Minvydas Ragulskis *

Research Group for Mathematical and Numerical Analysis of Dynamical Systems, Kaunas University of Technology, Studentu 50-222, Kaunas LT-51638, Lithuania

ARTICLE INFO

Article history:
Received 10 December 2010
Received in revised form 17 March 2011
Accepted 15 April 2011
Available online 30 April 2011

Keywords:
Averaging in time
Evolutionary algorithms
Moiré fringes
Visual cryptography

ABSTRACT

Image hiding based on time-averaged fringes produced by non-harmonic oscillations and near-optimal moiré gratings is presented in this paper. The secret image is embedded into the background moiré grating. Phase matching and initial stochastic phase scrambling algorithms are used to encrypt the image. The decoding of the image is completely visual. The embedded secret image appears when the encrypted image is oscillated in a predefined direction, according to a predefined law of motion. No secret is leaked when the encrypted image is oscillated harmonically at any amplitude of oscillation. The criterion of the optimality of a moiré grating serves as a fitness function for evolutionary algorithms which are used to identify a near-optimal moiré grating for image hiding applications. Numerical experiments are used to illustrate the functionality of the method.

1. Introduction

Visual cryptography is a cryptographic technique which allows visual information (pictures, text, etc.) to be encrypted in such a way that the decryption can be performed by the human visual system, without the aid of computers. Visual cryptography was pioneered by Naor and Shamir in 1994 [1]. They demonstrated a visual secret sharing scheme, where an image was broken up into n shares so that only someone with all n shares could decrypt the image, while any $n-1$ shares revealed no information about the original image. Each share was printed on a separate transparency, and decryption was performed by overlaying the shares. When all n shares were overlaid, the original image would appear.

Since 1994, many advances in visual cryptography have been done. An extended visual cryptography scheme is proposed in Ref. [2]. A new visual cryptography scheme for gray-level images based on dithering techniques is presented in Ref. [3]. A new secret image sharing scheme for true-color secret images is proposed in Ref. [4]. A multiple-level visual secret-sharing scheme without image size expansion is presented in Ref. [5]. Probabilistic $(2,n)$ visual secret sharing scheme for binary images is presented in Ref. [6]. A robust copyright protection scheme for digital image is proposed in Ref. [7]. In this scheme, the watermark does not require to be embedded into the protected image but is used to generate a secret image and a public image by using the visual cryptography technique. A user authentication scheme for visual secret sharing to ensure deliberate human interaction is presented in Ref. [8].

Geometric moiré [9,10] is a classical in-plane whole-field non-destructive optical experimental technique based on analysis of visual patterns produced by superposition of two regular gratings that geometrically interfere. Examples of gratings are equispaced parallel lines, concentric circles or arrays of dots.

Two basic goals exist in moiré pattern research. The first is the analysis of moiré patterns. The task is to analyze the distribution of moiré fringes and interpret experimentally produced patterns of fringes. Another goal is moiré pattern synthesis when the generation of a certain predefined moiré pattern is required.

The synthesis process involves production of two such images that the required moiré pattern emerges when those images are superimposed [11]. Moiré synthesis and analysis are tightly linked and understanding one task gives insight into the other. Conditions ensuring that a desired moiré pattern will be present in the superposition of two images are predetermined; however, they do not specify these two original images uniquely. The freedom in choosing the superimposed images can be exploited to produce various degrees of visibility and ensure the desired properties. Several criteria are proposed in Refs. [12,13] to resolve that freedom in moiré pattern synthesis.

The image hiding method based on time-averaging moiré is proposed in Ref. [14]. This method is based not on static superposition of moiré images, but on time-averaging geometric moiré. This method generates only one picture; the secret image can be interpreted by the naked eye only when the original encoded image is harmonically oscillated in a predefined direction at strictly defined amplitude of oscillation. This method, strictly speaking, is not a visual cryptography scheme. It resembles a visual cryptography scheme because one needs a computer to encode a secret, and one can decode the secret without a computing device. Only one picture is generated, and the secret is leaked from this picture when parameters of the oscillation are appropriately tuned. In other words, the secret can be decoded by trial

* Corresponding author. Tel.: +370 69822456; fax: +370 37330446.
E-mail addresses: edita.sakyte@ktu.lt (E. Sakyte), rita.palivonaite@ktu.lt (R. Palivonaite), algiment.aleksa@ktu.lt (A. Aleksa), minvydas.ragulskis@ktu.lt (M. Ragulskis).
URL: http://www.personalas.ktu.lt/~mragul (M. Ragulskis).

0030-4018/$ – see front matter © 2011 Elsevier B.V. All rights reserved.
doi:10.1016/j.optcom.2011.04.039

and error — if only one knows that he has to shake the slide. Therefore, additional image security measures are implemented in Ref. [14], particularly splitting of the encoded image into two shares. Oscillation of any of the shares separately does not reveal the secret. Two shares must be superimposed and then oscillated before the secret image can be interpreted.

The image encoding method which reveals the secret image not only at exactly tuned parameters of the oscillation, but also requires that the time function determining the process of oscillation must comply with specific requirements is developed in Ref. [15]. This image hiding method based on time-averaging moiré and non-harmonic oscillations does not reveal the secret image at any amplitude of harmonic oscillations. Instead, the secret is leaked only at carefully chosen parameters of this specific time function (when the density function of the time function is a symmetric uniform density function).

Stepped (black and white) moiré gratings are used in Ref. [15] to encode the secret image. The main objective of this paper is to determine if a better moiré grating exists compared to the stepped grating. The criteria for the optimality of the moiré grating are straightforward: no time-averaged fringes should develop when this grating is oscillated harmonically, and the secret image should be leaked when the grating is oscillated by the time function whose density function is a symmetric uniform density function.

This paper is organized as follows. Initial definitions are given in Section 2; the optimality criterion for a grayscale moiré grating is constructed in Section 3; perfect grayscale grating functions are defined in Section 4 applicability of evolutionary algorithms for the identification of a near-optimal moiré grating is discussed in Section 5; image hiding in near optimal perfect grayscale gratings is presented in Section 6; concluding remarks are given in Section 7.

2. Initial definitions and optical background

We will consider one-dimensional moiré gratings in this paper.

Definition 1. Function $F(x)$ is a grayscale grating function if the following requirements hold:

Requirement 1. The grating is a periodic function; $F(x+\lambda)=F(x)$; λ is the pitch of the grating.

Requirement 2. $0\le F(x)\le 1$; 0 corresponds to the black color, 1 corresponds to the white color and all intermediate numerical values of the grating correspond to an appropriate grayscale level.

Requirement 3. $F(x)$ has only a finite number of discontinuity points in every finite interval $[a, b]$; $a<b$ ($F(x)$ is an integrable function).

Example 1. A harmonic function

$$\tilde{F}(x)=\frac{1}{2}+\frac{1}{2}\sin\left(\frac{2\pi}{\lambda}x\right) \tag{1}$$

and a stepped function

$$\overline{F}(x)=\begin{cases} 1, \text{ when } x\in\left[\lambda j;\lambda\left(j+\frac{1}{2}\right)\right]; \\ 0, \text{ when } x\in\left(\lambda\left(j+\frac{1}{2}\right);\lambda(j+1)\right)\end{cases} \tag{2}$$

are used for the construction of grayscale grating functions for image hiding applications in Ref. [15]. In this paper we will use an m-pixel grayscale grating function $F_{m,n}(x)$ which is defined as follows:

$$F_{m,n}(x)=y_k \text{ when } \left(\frac{(k-1)\lambda}{m}+j\lambda\right)\le x\le\left(\frac{k\lambda}{m}+j\lambda\right);\ k=1,2,\ldots,m;\ j\in Z \tag{3}$$

where y_k, $k=1, 2,\ldots, m$ are grayscale levels assigned accordingly from a set of discrete grayscale levels comprising n elements distributed uniformly in the interval [0;1]. The pixel's length (in one-dimensional coordinate system) is $\frac{\lambda}{m}$; m pixels fit into the period of the grayscale grating function. For example, $F_{22,256}(x)$ represents a grayscale grating function the period of which accommodates 22 pixels and the grayscale level of every pixel can be selected from 256 different levels.

We will use following parameters for the characterization of grayscale grating functions:

$$\text{i. } \overline{C}=\sup F(x); \tag{4}$$

$$\text{ii. } \underline{C}=\inf F(x); \tag{5}$$

$$\text{iii. } \gamma=\frac{1}{\lambda}\int_0^{\lambda}F(z)dz; \tag{6}$$

$$\text{iv. } \|F(x)\|=\frac{1}{\lambda}\int_0^{\lambda}\left|F(z)-\frac{1}{2}\right|dz. \tag{7}$$

Following relationships hold:

$$1.\ 0\le\underline{C}\le F(x)\le\overline{C}\le 1;\ x\in R. \tag{8}$$

$$2.\ 0\le\|F(x)\|\le\left|\gamma-\frac{1}{2}\right|. \tag{9}$$

3. $F(x)$ can be expanded into the Fourier series:

$$F(x)=\frac{a_0}{2}+\sum_{k=1}^{\infty}\left(a_k\cos\frac{2\pi kx}{\lambda}+b_k\sin\frac{2\pi kx}{\lambda}\right);\ a_k,b_k\in R; \tag{10}$$
$$k=1,2,\ldots;\ a_0=2\gamma.$$

Example 2. Coefficients of the Fourier expansion and parameters for different grayscale grating functions read:

1. For the harmonic grayscale grating function $\tilde{F}(x)$:

$$a_0=1\ ;\ a_1,a_2,a_3,\ldots=0\ ;\ b_1=\frac{1}{2}\ ;\ b_2,b_3,\ldots=0\ ; \tag{11}$$
$$\overline{C}=1\ ;\ \underline{C}=0\ ;\ \gamma=\frac{1}{2}\ ;\ \left\|\tilde{F}(x)\right\|=\frac{1}{\pi}.$$

2. For the stepped grayscale grating function $\overline{F}(x)$:

$$a_0=1\ ;\ a_1,a_2,a_3,\ldots=0\ ;\ b_k=\frac{1+(-1)^{k+1}}{k\cdot\pi}\ ; \tag{12}$$
$$k=1,2,\ldots;\ \overline{C}=1\ ;\ \underline{C}=0\ ;\ \gamma=\frac{1}{2}\ ;\ \left\|\overline{F}(x)\right\|=\frac{1}{2}.$$

3. For the m-pixels grayscale grating function $F_{m,n}(x)$:

$$a_0=\frac{2}{m}\sum_{k=1}^{m}y_k\ ;\ a_k=\frac{1}{k\pi}\sum_{j=1}^{m}\left(\left(y_{j-1}-y_j\right)\sin\frac{2(j-1)k\pi}{m}\right);$$
$$b_k=-\frac{1}{k\pi}\sum_{j=1}^{m}\left(\left(y_{j-1}-y_j\right)\cos\frac{2(j-1)k\pi}{m}\right)\ ;\ k=1,2,\ldots; \tag{13}$$
$$\overline{C}=\max_k y_k\ ;\ \underline{C}=\min_k y_k\ ;\ \gamma=\frac{1}{m}\sum_{k=1}^{m}y_k\ ;\ \left\|F_{m,n}(x)\right\|$$
$$=\frac{1}{m}\sum_{k=1}^{m}\left(y_k-\frac{1}{2}\right).$$

Definition 2. The time averaging operator H_s is defined as [16]:

$$H_s(x|F;\xi_s) = \lim_{T\to\infty}\frac{1}{T}\int_0^T F(x-\xi_s(t))dt \tag{14}$$

where t is time; T is the exposure time; $\xi_s(t)$ is a function describing dynamic deflection from the state of equilibrium; s is a real parameter; $s\geq 0$; $x\in R$.

In this paper we will use two different time functions $\xi_s(t)$. The first one describes the process of harmonic oscillations:

$$\tilde{\xi}_s(t) = s\sin(\omega t+\varphi), \tag{15}$$

where s is the amplitude; ω is the angular frequency and φ is the phase of harmonic oscillations. Another time function describes the zig-zag type oscillations:

$$\hat{\xi}_s(t) = \begin{cases} \frac{2s\omega}{\pi}\left(t-\left(\frac{2\pi}{\omega}j-\frac{\pi}{2\omega}\right)\right)-s, \\ \text{when}\left(\frac{2\pi}{\omega}j-\frac{\pi}{2\omega}\right)\leq t\leq\left(\frac{2\pi}{\omega}j+\frac{\pi}{2\omega}\right) \\ -\frac{2s\omega}{\pi}\left(t-\left(\frac{2\pi}{\omega}j+\frac{\pi}{2\omega}\right)\right)+s, \\ \text{when}\left(\frac{2\pi}{\omega}j+\frac{\pi}{2\omega}\right)\leq t\leq\left(\frac{2\pi}{\omega}j+\frac{3\pi}{2\omega}\right) \end{cases}, \tag{16}$$

where s is the amplitude; ω is the frequency and φ is the phase of zig-zag oscillations. Both functions can be easily implemented experimentally — any shaker table with appropriate control instrumentation can execute harmonic and zig-zag oscillations.

In Ref. [15] it is shown that:

i. $$H_s\left(x|F;\tilde{\xi}_s\right) = \frac{a_0}{2} + \\ + \sum_{k=1}^{\infty}\left(a_k\cos\frac{2\pi kx}{\lambda}+b_k\sin\frac{2\pi kx}{\lambda}\right)J_0\left(\frac{2\pi k}{\lambda}s\right); \tag{17}$$

ii. $$H_s\left(x|F;\hat{\xi}_s\right) = \frac{a_0}{2} + \\ + \sum_{k=1}^{\infty}\left(a_k\cos\frac{2\pi kx}{\lambda}+b_k\sin\frac{2\pi kx}{\lambda}\right)\frac{\sin\left(\frac{2\pi k}{\lambda}s\right)}{\left(\frac{2\pi k}{\lambda}s\right)}; \tag{18}$$

where J_0 is zero order Bessel function of the first kind.

Example 3.

$$H_s\left(x|\tilde{F};\tilde{\xi}_s\right) = \frac{1}{2}+\frac{1}{2}\sin\left(\frac{2\pi}{\lambda}x\right)J_0\left(\frac{2\pi}{\lambda}s\right). \tag{19}$$

The proof follows immediately from Eq. (17). It can be noted that this is a well known result in optical engineering. A time averaged geometric moiré fringe is formed at such amplitudes of harmonic oscillations where $J_0\left(\frac{2\pi}{\lambda}s\right)=0$. In other words, the explicit relationship between the amplitude of harmonic oscillation, the pitch of the grating and the order of the time-averaged fringe takes the following form:

$$\frac{2\pi}{\lambda}s_n = r_n;\ n=1,2,\ldots \tag{20}$$

where the fringe order n is determined using manual, semi-manual or fully automatic fringe enumeration techniques [9].

Definition 3. The mean of a time-averaged grayscale grating function is defined as:

$$E(H_s(x|F,\xi_s)) = \frac{1}{\lambda}\int_0^{\lambda} H_s(x|F,\xi_s)dx; \tag{21}$$

where E is the averaging operator.

Corollary 1.

$$E\left(H_s\left(x|F,\tilde{\xi}_s\right)\right) = E\left(H_s\left(x|F,\hat{\xi}_s\right)\right) = \frac{a_0}{2} = \gamma. \tag{22}$$

The proof follows from Eqs. (17) and (18).

Definition 4. The standard deviation of a time-averaged grayscale grating function is:

$$\sigma(H_s(x|F;\xi_s)) = \sqrt{\frac{1}{\lambda}\int_0^{\lambda}(H_s(x|F;\xi_s)-E(H_s(x|F;\xi_s)))^2dx}. \tag{23}$$

Corollary 2. The standard deviation of a grayscale grating function oscillated harmonically reads:

$$\sigma\left(H_s\left(x|F;\tilde{\xi}_s\right)\right) = \frac{\sqrt{2}}{2}\sqrt{\sum_{k=1}^{\infty}(a_k^2+b_k^2)J_0^2\left(\frac{2\pi ks}{\lambda}\right)}. \tag{24}$$

Moreover,

$$\sigma\left(H_s\left(x|\tilde{F};\tilde{\xi}_s\right)\right) = \frac{\sqrt{2}}{4}\cdot\left|J_0\left(\frac{2\pi}{\lambda}s\right)\right|. \tag{25}$$

But the standard deviation of a grayscale grating function oscillated by a zig-zag time function reads:

$$\sigma\left(H_s\left(x|F;\hat{\xi}_s\right)\right) = \frac{\sqrt{2}\lambda}{4\pi\cdot s}\sqrt{\sum_{k=1}^{\infty}(a_k^2+b_k^2)\frac{\sin^2\left(\frac{2\pi ks}{\lambda}\right)}{k^2}}. \tag{26}$$

Corollary 3. $\inf_s\left(\sigma\left(H_s\left(x|F;\hat{\xi}_s\right)\right)\right)=0$ for any grayscale grating function.

Proof. It is clear that $\sigma\left(H_s\left(x|F;\hat{\xi}_s\right)\right)\geq 0$. The equality $\sigma\left(H_s\left(x|F;\hat{\xi}_s\right)\right)=0$ will hold when $\sin\left(\frac{2\pi ks}{\lambda}\right)=0$ and $s\neq 0$ for every $k=1,2,\ldots$ (Eq. (26)). For a fixed k the last condition yields $s_n=\frac{\lambda}{2k}n$; $n=1,2,\ldots$. But since the sine function is a periodic function, $\sin\left(\frac{2\pi ks}{\lambda}\right)$ becomes equal to zero at $s_m=\frac{\lambda}{2}m$; $m=1,2,\ldots$ for all k. *End of Proof.*

These effects are illustrated in Fig. 1. Time-averaged fringes generated by a harmonic grating function oscillated harmonically are shown in Fig. 1(a); the solid line and black circles in Fig. 1(b) illustrate the zero order Bessel function of the first kind $J_0\left(\frac{2\pi}{\lambda}s\right)$ and its roots. Time-averaged fringes produced by a non-harmonic grating function oscillated by a zig-zag function are shown in Fig. 1(c); the dashed line and empty circles in Fig. 1(b) illustrate the function $\frac{\sin\left(\frac{2\pi}{\lambda}s\right)}{\frac{2\pi}{\lambda}s}$ and its roots.

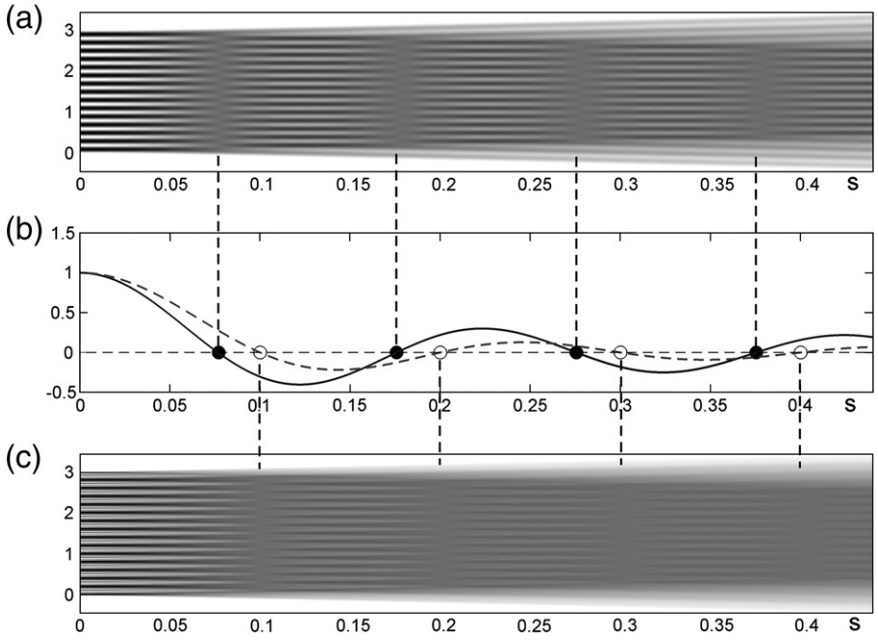

Fig. 1. Patterns of time-averaged fringes produced by a harmonic moiré grating ($\lambda = 0.1$) oscillated harmonically (a) and by a non-harmonic grating oscillated by a "zig-zag"-type time function (c). The line drawing in part (b) illustrates appropriate envelope functions and their roots; vertical dashed lines mark centerlines of corresponding time-averaged fringes.

Corollary 4. $\inf_s\left(\sigma\left(H_s\left(x|F;\ \tilde{\xi}_s\right)\right)\right) = 0$ if and only $F(x) \equiv \tilde{F}(x)$ or $F(x) = c$ for all x; $0 \le c \le 1$.

Proof. It is clear that $\sigma\left(H_s\left(x|F;\ \tilde{\xi}_s\right)\right) = 0$ when $F(x) = c$ for all x. Otherwise, the equality $\sigma\left(H_s\left(x|F;\ \tilde{\xi}_s\right)\right) = 0$ will hold when $J_0\left(\frac{2\pi k s}{\lambda}\right) = 0$ for every $k = 1, 2,\ldots$ (Eq. (24)). For a fixed k the last condition yields $s_n = \frac{\lambda}{2\pi k} r_n$; $n = 1, 2,\ldots$; where r_n is the n-th root of J_0. But roots of the zero order Bessel function of the first kind are distributed not uniformly [17]. Thus it is impossible to find such recurrent values of s_n where $J_0\left(\frac{2\pi k s}{\lambda}\right) = 0$ for every $k = 1, 2,\ldots$. This fact is illustrated in Fig. 2; values of $s_n = \frac{\lambda}{2\pi k} r_n$; $n = 1, 2,\ldots$ at fixed k are marked as empty circles on the horizontal dashed lines.

If $F(x)$ is a harmonic function, $a_1^2 + b_1^2 > 0$; but $a_k^2 + b_k^2 = 0$ for all $k = 2, 3,\ldots$ (λ is equal to the wavelength of the harmonic function). Then, $\inf_s\left(\sigma\left(H_s\left(x|F;\ \tilde{\xi}_s\right)\right)\right) = 0$ for $s_n = \frac{\lambda}{2\pi} r_n$; $n = 1, 2,\ldots$ (compare to Example 3). *End of proof.*

3. The construction of the optimality criterion for $F_{m,n}(x)$

The results of Corollaries 3 and 4 are used in Ref. [15] for hiding an image in a stepped moiré grating. Since coefficients of the Fourier expansion of a stepped moiré grating are described by Eq. (12), Corollary 4 yields:

$$\inf_s\left(\sigma\left(H_s\left(x|\bar{F};\ \tilde{\xi}_s\right)\right)\right) > 0. \tag{27}$$

In other words, time-averaged moiré fringes will not develop when a stepped moiré grating is oscillated harmonically at any amplitude of oscillations and the embedded secret image cannot be decrypted by

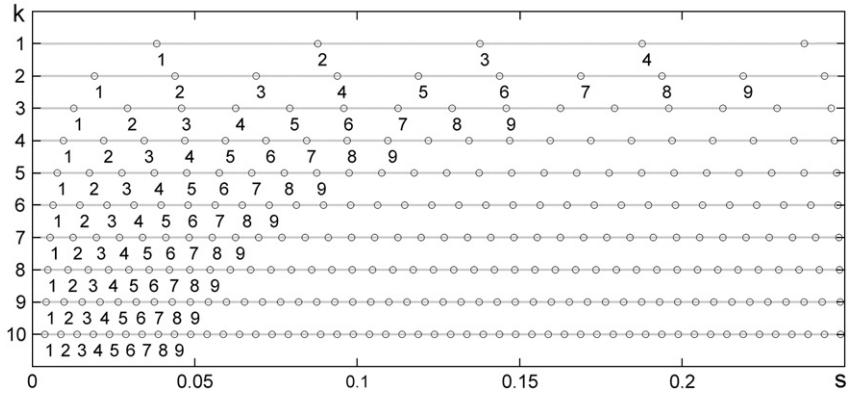

Fig. 2. Distribution of centers of time-averaged fringes for different harmonic components of Fourier expansion of a moiré grating oscillated harmonically; only the first nine roots are numbered for clarity.

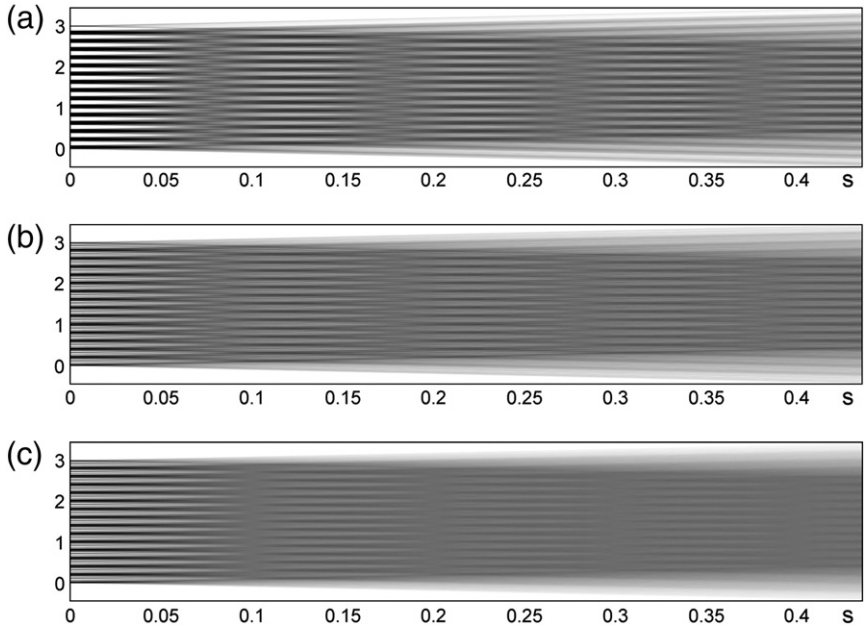

Fig. 3. Undeveloped time-averaged fringes produced by the stepped moiré grating (a) and the near-optimal moiré grating (b); the pitch of both gratings is $\lambda = 0.1$; both gratings are oscillated harmonically. Full time-average fringes develop when the near-optimal moiré grating is oscillated by a "zig-zag" time function (c).

harmonic oscillations (Fig. 3). Zig-zag oscillations, on the contrary, enable effective visual decryption of the secret image [15].

Therefore the magnitude $\inf_s\left(\sigma\left(H_s\left(x|F;\ \tilde{\xi}_s\right)\right)\right)$ can be considered as a measure of the quality of the encryption. The higher is this number, the harder is to interpret the embedded image when it is oscillated harmonically. Then the following question arises. Is the stepped moiré grating $\overline{F}(x)$ an optimal grating (in the sense described above)? Maybe it is possible to find another grayscale grating function for which the lowest value of the standard deviation of the time-averaged image produced by harmonic oscillations is higher compared to the stepped moiré grating. Finding the answer to this question is the primary objective of this paper.

As mentioned previously, we will seek a grayscale grating function for which the lowest value of the standard deviation of the time-averaged image produced by harmonic oscillations is maximal. Unfortunately, this is a very complex problem of variational optimization. But we consider digital representations of grayscale grating functions. In other words, we will operate with m-pixel grayscale grating functions only. That simplifies the optimization problem considerably.

Also, it can be noted that it is not likely that very large amplitudes ($s>\lambda$) would be used for the decryption of the embedded image [14,15]. Thus we further simplify the optimization problem — the minimal value of the standard deviation will be sought in the interval of amplitudes S_1 surrounding the amplitude $\frac{\lambda r_1}{2\pi}$ at which $\sigma\left(H_s\left(x|\ \tilde{F}\ ;\ \tilde{\xi}_s\right)\right)$ reaches its first minimum:

$$S_1 := \left[\frac{\lambda r_1}{2\pi} - \frac{\lambda(r_2 - r_1)}{4\pi}; \frac{\lambda r_1}{2\pi} + \frac{\lambda(r_2 - r_1)}{4\pi}\right]. \tag{28}$$

The variation of standard deviations of $\tilde{F}(x)$ and $\overline{F}(x)$ in the interval S_1 is illustrated in Fig. 4.

Definition 5. The optimality criterion $\delta(F)$ for a grayscale grating function F is defined as follows:

$$\delta(F) = \min_{s\in S_1}\left(\sigma\left(H_s\left(x|F;\ \tilde{\xi}_s\right)\right)\right). \tag{29}$$

It is clear that $\delta(\tilde{F}) = 0$. On the other hand, $\delta(\overline{F}) = 0.0467$ (at $s_{\min} = 0.2744$; Fig. 4) is the lower bound of the optimization procedure.

4. Perfect grayscale grating functions

The optimization problem $\max_{\forall F_{m,n}}(\delta(F))$ could be commenced, but we introduce the definition of a perfect grayscale grating function first.

Definition 6. $F(x)$ is a perfect grayscale grating function if four additional requirements hold true besides the requirements raised in the Definition 1:

Requirement 4. The grating spans through the whole grayscale interval: $\overline{C} = 1$; $\underline{C} = 0$.

Requirement 5. The average grayscale level in a pitch of the grating equals to exactly the middle grayscale level between the white and the black colors: $\gamma = 0.5$.

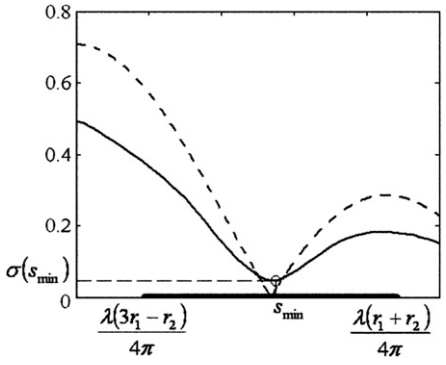

Fig. 4. The variation of standard deviations of the harmonic grayscale grating function (the dashed line) and the stepped grayscale grating function (the thin solid line) oscillated harmonically; the thick solid line on the s-axis denotes the interval S_1; the empty circle denotes the amplitude $s_{\min}$ where the standard deviations $\sigma\left(H_{s_{min}}\left(x|\overline{F};\ \tilde{\xi}_s\right)\right)$ of the time-averaged image reaches its minimum in S_1.

Requirement 6. The norm of the grayscale grating function must be at least equal to the half of the norm of the harmonic grayscale grating: $\|F(x)\| \geq \frac{1}{2}\|\tilde{F}(x)\| = \frac{1}{\pi}$.

Requirement 7. The pitch of the grating λ must be easily identifiable. The main peak of the discrete Fourier amplitude spectrum at $\frac{2\pi}{\lambda}$ must be at least two times higher compared to all other peaks: $\sqrt{a_1^2 + b_1^2} \geq 2\sqrt{a_j^2 + b_j^2}$ for all $j = 2, 3, \ldots$.

The necessity of the introduction of perfect grayscale grating functions is reasoned by the peculiarities of the decryption procedure and the formation of time averaged moiré fringes (Fig. 5). Requirement 4 forces to use the whole range of discrete grayscale levels. Requirement 5 demands that the grayscale level in the center of a time-averaged fringe is equal to 0.5. Requirement 6 does not allow grayscale functions which slightly vary around 0.5 and have only few black and white pixels in a pitch of the grating. Requirement 7 demands that the pitch of a grating must be clearly visible by a naked eye. Otherwise, parasitic time averaged moiré fringes may form at different amplitudes if, for example, the second peak of the discrete Fourier amplitude spectrum at $\frac{4\pi}{\lambda}$ is comparable to the main peak at $\frac{2\pi}{\lambda}$.

Corollary 5. $\tilde{F}(x)$ and $\bar{F}(x)$ are perfect grayscale functions.

Proof. The proof for $\tilde{F}(x)$ is trivial. The proof for $\bar{F}(x)$ is also straightforward: $\|\bar{F}(x)\| = \frac{1}{2} > \frac{1}{\pi}$, thus Requirement 6 holds. Coefficients of the Fourier expansion of $\bar{F}(x)$ read: $a_0, a_1, a_2, \ldots = 0$; $b_{2k-1} = \frac{2}{(2k-1)\cdot\pi}$; $b_{2k} = 0$; $k = 1, 2, \ldots$ (Eq. (12)). So, $b_1 = \frac{2}{\pi}$; but $|b_k| \leq \frac{2}{\pi k}$; $k = 2, 3, \ldots$. Thus, Requirement 7 holds also. *End of proof.*

It is clear that $F_{m,n}(x)$ is not necessarily a perfect grayscale grating function.

Stepped grayscale grating functions comprising 22 pixels in the pitch of the grating are used to encode digital images in Ref. [15]. We will also use 22 pixels in the pitch of the grating; $m = 22$. Also, we assume only 32 different discrete grayscale levels (instead of 256) in order to reduce the capacity of the problem even more. In other words, all possible discrete grayscale levels of y_k can be enumerated as $\frac{j}{31}$; $j = 0, 1, 2, \ldots, 31$.

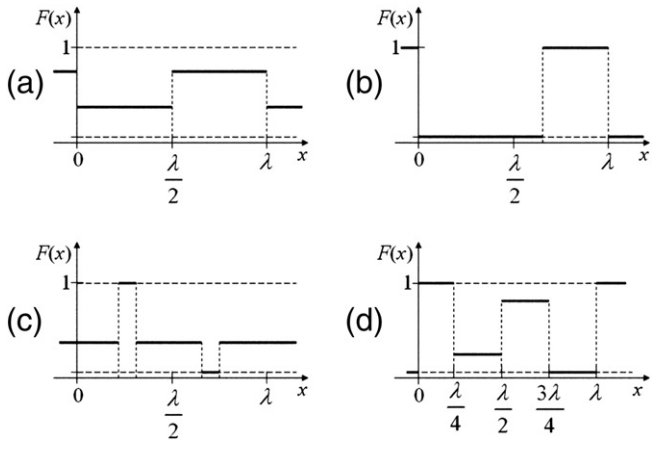

Fig. 5. Illustrations of not perfect grayscale grating functions: (a) — Requirement 4 does not hold; the whole range of grayscale levels is not used; (b) — Requirement 5 does not hold; the average grayscale level in a pitch does not equal to 0.5; (c) — Requirement 6 does not hold; the norm of the grayscale grating function is too small; (d) — Requirement 7 does not hold; the secondary harmonic is too high.

Now, finding an optimal perfect 22-pixel grayscale grating function is a straightforward task. One must generate all possible functions $F_{22,32}(x)$ and check if a currently generated function is perfect. If it is a perfect function, one needs to compute $\delta(P_{22,32})$. The highest value of $\delta(P_{22,32})$ produced after the full sorting algorithm will correspond to the optimal moiré grating. Unfortunately, this full sorting strategy is unrealistic due to the limited computational resources even after the above-mentioned simplifications and reductions. Naturally, the alternative objective is to seek near-optimal moiré gratings. We will use evolutionary algorithms for that purpose.

5. The construction of evolutionary lgorithms

We construct an evolutionary algorithm in such way that every chromosome represents one period of a grayscale function $F_{22,32}(x)$. The length of each chromosome is 22; every gene is an integer number between 0 and 31. The value of each gene represents a grayscale level for the respective pixel. The fitness of a chromosome is estimated by calculating $\delta(F_{22,32})$ (Eq. (28)). Since we operate with perfect moiré gratings only, the fitness function $\Phi(F_{22,32})$ takes the following form:

$$\Phi\left(F_{22,32}\right) = \begin{cases} 0 \text{ if } F_{22,32}(x) \text{ is not perfect;} \\ \delta\left(F_{22,32}\right) \text{ if } F_{22,32}(x) \text{ is perfect.} \end{cases} \quad (30)$$

The initial population comprises n randomly generated chromosomes with values of genes uniformly distributed over the interval [0; 31]. The fitness of each perfect chromosome is evaluated and an even number of chromosomes is selected to the mating population. We use a random roulette method for the selection of chromosomes. The chance that the chromosome will be selected to the mating population is proportional to its fitness value. Nevertheless, a probability that a chromosome with a low fitness value will be selected is not zero. Also, several copies of the same chromosome are allowed. All chromosomes are paired when process of mating is over.

The crossover between two chromosomes is executed for all pairs in the mating population. We use one-point crossover method and the location of this point is random. We also introduce a crossover coefficient κ which characterizes a probability that the crossover procedure will be executed for a pair of chromosomes.

In order to avoid convergence to one local solution a mutation procedure is used. The mutation parameter μ ($0 < \mu < 1$) determines the probability for a chromosome to mutate. The quantity of chromosomes which are exposed to the mutation procedure is calculated as $n_m = round(\mu \cdot n)$. Then n_m chromosomes are selected randomly and one gene of each chromosome is changed by a random number $\mathrm{mod}_{32}(\tau + r)$; here τ is the gene value before the modification; r is a random integer uniformly distributed over the interval [0; 31].

In general, the selection of parameters of evolutionary algorithms is an empirical process, though some common principles are described in Ref. [18], [19]. The following parameters of the evolutionary algorithm must be pre-selected: the crossover coefficient κ; the mutation parameter μ; the size of the population n and the number of generations. We will use recommendations for a classical model of an evolutionary algorithm [18]. The crossover coefficient κ will be selected from an interval [0.6; 0.8] and the mutation parameter μ from an interval [0; 0.3].

There are no definitive methods of establishing how many generations an evolutionary algorithm should run for. Simple problems may converge on good solutions after only 20 or 30 generations. More complex problems may need more. It is not unusual to run an evolutionary algorithm for 400 generations for more complex problems such as jobshops [20]. The most reliable method of deciding on this is trial and error, although a number of authors have suggested methods for determining how long a solution

should live [18], [20]. We will use 40 generations in our model, since further increase of the number of generations does not show improvement in the number of successful trials.

In order to tune numerical values of parameters κ and μ we construct an artificial problem — we seek a best perfect grayscale grating function $F_{6,5}(x)$ (comprising 6 pixels in a period; each pixel can acquire one of 5 discrete grayscale levels). Computational costs of a full sorting algorithm for a problem of such size are not high. Grayscale levels of the best perfect grayscale grating are: $\frac{1}{4}\cdot[0\ \ 1\ \ 0\ \ 4\ \ 3\ \ 4]$; the fitness of this function is $\Phi=0.057831$.

A single execution of an evolutionary algorithm produces one grayscale grating function. Clearly, the fitness of the generated function cannot be higher than 0.057831. On the other hand, the outcome depends on the initial population of chromosomes (among other random factors). Therefore, we execute the evolutionary algorithm (at fixed values of parameters) for 10 times and calculate how many times the fitness of the produced grayscale grating function is equal to 0.057831 (the number of successful trials is denoted by k). As mentioned previously, the fitness is calculated only for perfect grayscale grating functions (Eq. (30)). For example, the objective parameter δ of the grating $\frac{1}{4}\cdot[4\ \ 4\ \ 0\ \ 2\ \ 0\ \ 4]$ is $0.0587>0.057831$, but its fitness is set to zero because this grating is not perfect.

It can be noted that only about 7.8% of all grayscale grating functions $F_{6,5}(x)$ are perfect grayscale grating functions. A random population of 500 chromosomes yields in average 39 perfect gratings. We fix $n=500$ (both the mating, initial and the current population). Simulation results are presented in Table 1; $E(\Phi(F_{6,5}))$ denotes average fitness function calculated for 10 trials. Initially we fix $\mu=0.05$ and perform experiments with $\kappa=0.6$, 0.7 and 0.8. The number of successful trials is highest at $\kappa=0.7$; moreover the highest $\Phi(F_{6,5})$ is also produced at $\kappa=0.7$. We continue with $\mu=0.01$, 0.1, 0.2 and 0.3 (at $\kappa=0.7$). Best results are produced at $\mu=0.3$ (Table 1).

The fact that the fitness is calculated only for perfect grayscale grating functions and that only a low average percentage of perfect functions exist in the initial random population poses a threat that the evolutionary algorithm will converge to local maximum without spanning the whole set of perfect grayscale grating functions. Therefore we modify the mutation procedure introducing the incremental magnification of the parameter μ in every consecutive generation. The first generation starts with $\mu=0.05$ and is gradually increased up to 0.5 in the final generation. Though the number of successful trials is the same compared to the same experiment at $\kappa=0.7$ and $\mu=0.3$, the maximum fitness of the best perfect grating is considerably higher (Table 1).

We fix values of parameters of the evolutionary algorithm ($\kappa=0.7$ and incremental increase of μ from 0.05 till 0.5) and continue with grayscale grating functions comprising 22 pixels and 32 discrete grayscale levels, but the size of the population is $n=20000$ and the number of generations is 10 now. The evolutionary algorithm is executed 5 times; the best generated perfect grating is selected then. The near optimal perfect grayscale grating function $F_{22,32}(x)$ is shown in Fig. 7(a).

Table 1
The number of successful trials k and the average fitness function $E(\Phi(F_{6,5}))$ for different values of the crossover coefficient κ and the mutation parameter μ.

κ	μ	$E(\Phi(F_{6,5}))$	k
0.6	0.05	0.0505	3
0.7	0.05	0.0521	4
0.8	0.05	0.0507	3
0.7	0.01	0.0516	3
0.7	0.1	0.0521	4
0.7	0.2	0.0541	6
0.7	0.3	0.0549	7
0.7	[0.05; 0.5]	0.055	7

6. Image hiding in near optimal perfect grayscale gratings

As mentioned in previously, the goal of this paper is to find an optimal perfect grayscale grating which can be effectively used for image hiding based on time-averaged moiré fringes produced by zig-zag type oscillations. The secret image should be leaked in a form of a pattern of time-averaged moiré fringes when the encoded original image is oscillated in a predefined direction at strictly defined amplitude of zig-zag type oscillation (Fig. 3(c)). Moreover, the secret image should not be revealed at any amplitude of harmonic oscillations. The basic goal remains similar to objectives raised in Ref. [15]. The main difference now is in the structure of the grayscale grating which holds the embedded secret image. A stepped grayscale grating does not produce a time-averaged moiré fringe at any amplitude of harmonic oscillations [15]. But a stepped grayscale grating yields an array of undeveloped time-averaged fringes when the amplitude of harmonic oscillations sweeps over a preset frequency range. Of course, such undeveloped fringes cannot be used for image hiding applications — it would be hard to interpret the embedded image even at preselected amplitude of harmonic oscillations. Anyway, the near-optimal perfect grayscale grating $F_{22,32}(x)$ can be considered as a strong advancement of the security of the encryption — the undeveloped time-averaged fringes produced by harmonic oscillations are even less interpretable (Fig. 3(b)). What is even more important, the slope of the undeveloped fringe produced by $F_{22,32}(x)$ is much smaller compared to the slope of the undeveloped fringe produced by the stepped grayscale grating (Fig. 6).

It can be noted that two different gratings are used to embed a secret image into the background image [14,15]; one pitch of the grating is used to form the background of the secret image; another pitch is exploited to form the zones inherent to the secret image. We will use the near optimal grayscale grating $F_{22,32}(x)$ for the background; the pitch of this grating is $\lambda_0=1.76$ mm (22 pixels fit into 1.76 mm). It is clear that we cannot change the pitch of $F_{22,32}(x)$ without changing the size of each 22 pixels forming the near optimal grayscale grating; we change the number of pixels in the grating instead. The procedure is straightforward — the grayscale grating used for the secret image is constructed from $F_{22,32}(x)$ by deleting one pixel (the pitch then becomes $\lambda_1 = 1.76\cdot\frac{21}{22} = 1.64\,\text{mm}$). The produced grayscale grating $F_{21,32}(x)$ must be a perfect grayscale grating, thus we delete the pixel which numerical grayscale value is nearest 0.5 (Fig. 7B).

The secret image which will be embedded into the background moiré grating is illustrated in Fig. 8. The encoded secret image is shown

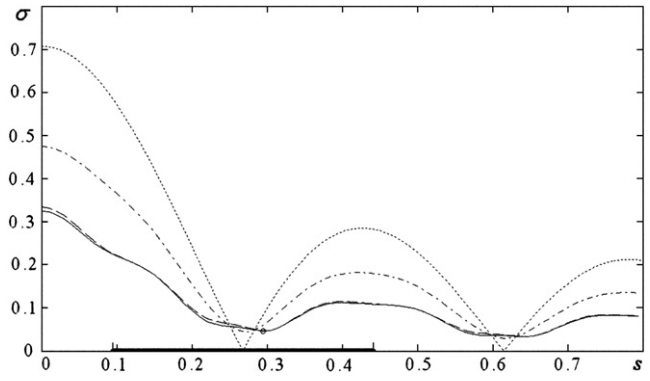

Fig. 6. The variation of standard deviations of grating functions oscillated harmonically: the dotted line represents the harmonic grayscale grating function; dotted-dashed line — the stepped grayscale grating function; thin solid line — the optimal perfect grayscale grating function $F_{6,5}(x)$ ([0 1 0 4 3 4]/4); dashed line — the optimal not perfect grayscale grating function $F_{6,5}(x)$ ([4 4 0 2 0 4]/4). The thick solid line on the s-axis denotes the interval S_1; the empty circle denotes the amplitude where the standard deviation of the time-averaged perfect grayscale grating function reaches its minimum in S_1.

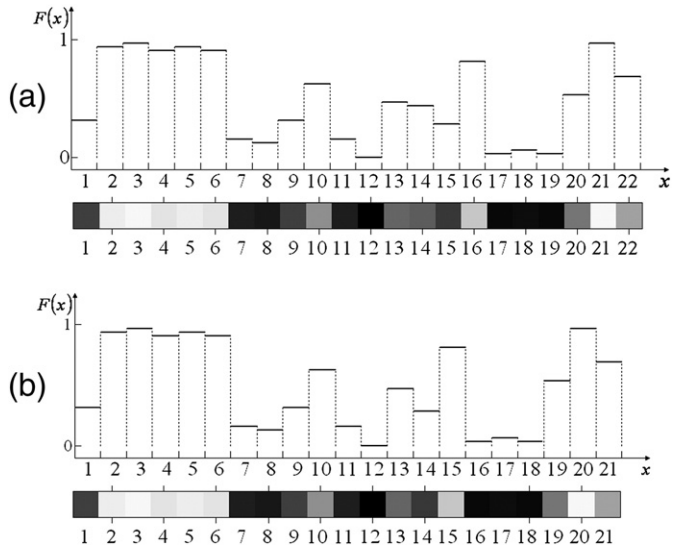

Fig. 7. Near optimal perfect grayscale grating functions $F_{22,32}(x)$ (a) and $F_{21,32}(x)$ (b) represented in line graphs and in grayscale level charts.

in Fig. 9; the size of the digital image is 80×48 mm (1890×1134 pixels); the pitch of the background moiré grating is $\lambda_0 = 1.76$ mm; the pitch at zones inherent to the secret image is $\lambda_1 = 1.68$ mm. Stochastic initial phase deflection and phase regularization algorithms [15] are used to hide the secret image into the background.

The secret image can be decrypted when the encoded image is oscillated by a zig-zag type time function. The secret image can be visualized in two alternative ways. Time-averaged moiré fringe forms at the region occupied by the secret image and it appears in a form of a gray even zone in a noisy background when the amplitude of zig-zag oscillation is $s = \frac{\lambda_1}{2} = 0.84\,\text{mm}$ (Fig. 10). It can be noted that time-averaged moiré fringes will form too when the amplitude of zig-zag oscillations will be $s_j = \frac{j\lambda_1}{2}, j = 2, 3, \ldots$. However the small elements of the secret image may disappear in the time-averaged image at higher amplitudes of oscillations. Alternatively, the background turns into a time-averaged moiré fringe and the secret image is leaked as a noisy area in the even background at $s = \frac{\lambda_0}{2} = 0.88\,\text{mm}$ (Fig. 11). Of course, the contrast of time-averaged moiré fringes can be enhanced using special algorithmic techniques [21] (Fig. 12), but the decryption can be performed by the human visual system, without the aid of computers. The secret image can be interpreted by a naked eye when the frequency of oscillations is high enough and the human visual system cannot follow rapidly oscillating objects [14]. It can be noted that the frequency of oscillations does not have any influence to the process of decryption (Eqs. (17) and (18)). Visual decryption is determined only by the amplitude of oscillations and the time function controlling the trajectory of motion in one period of oscillations.

The secret image cannot be leaked when the amplitude of "zig-zag" oscillations in not pre-selected accordingly; the time-averaged

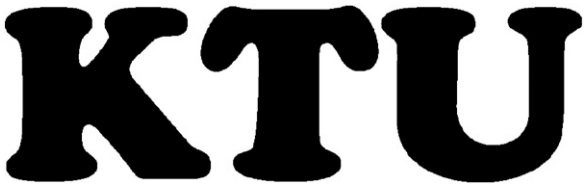

Fig. 8. The secret image.

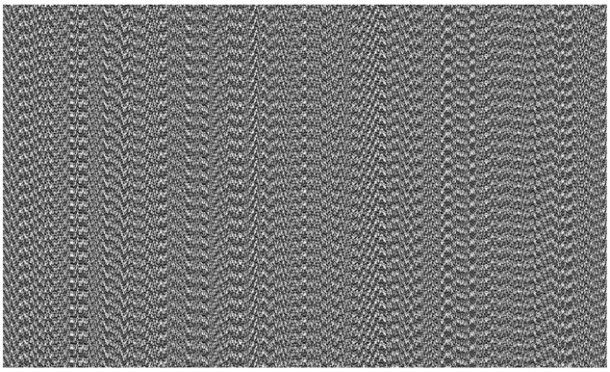

Fig. 9. The secret image encoded into the background moiré grating.

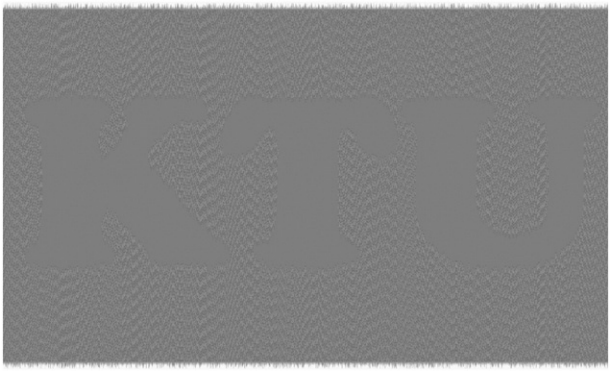

Fig. 10. Computational decryption of the secret image when the encoded image is oscillated by a "zig-zag" type time function at $s = \frac{\lambda_1}{2} = 0.84\,\text{mm}$.

image at $s = 1.04$ mm is shown in Fig. 13. Moreover, the secret image cannot be leaked if the encoded image is oscillated harmonically. This statement holds for any amplitude of harmonic oscillations. The time averaged image at $s = \frac{r_1\lambda_1}{2\pi} = 0.6433\,\text{mm}$ (here s denotes the amplitude of harmonic oscillations) is shown in Fig. 14.

7. Comparisons with existing image hiding techniques based on geometric moiré

Whenever a new technique is proposed for image hiding application, it is natural to expect comparisons with analogous existing techniques. Our technique is based on visual interpretation of moiré gratings. Thus we compare our method with the image

Fig. 11. Computational decryption of the secret image when the encoded image is oscillated by a "zig-zag" type time function at $s = \frac{\lambda_0}{2} = 0.88\,\text{mm}$.

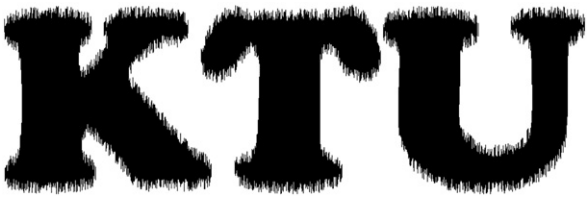

Fig. 12. Contrast enhancement of the decrypted image.

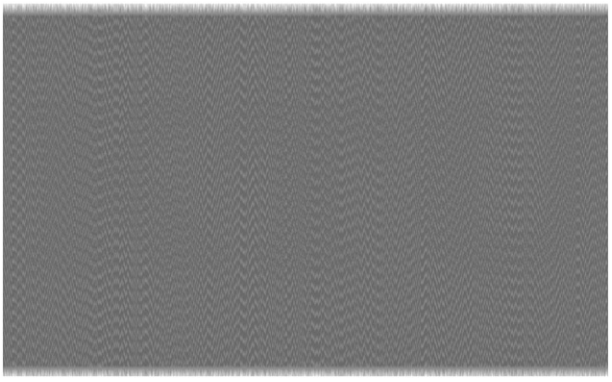

Fig. 13. The secret image cannot be leaked when the amplitude of "zig-zag" type oscillations in not pre-selected accordingly; the time-averaged image is shown at $s = 1.04$ mm.

encryption — decryption method based on geometric moiré where the intensity image is added as a reflectance map as an argument to the harmonic fringe pattern [22,23].

Though all compared methods exploit the phenomenon of geometric moiré, there exist distinct features which separate our method technique from the aforementioned methods. First of all, our method is based on time average moiré, not on a static superposition of moiré gratings which is exploited in Refs. [22,23]. We do not generate two or more shares which have to be overlapped. Our method is a one-image method; the encrypted image is not overlapped with any other image. On the contrary, the single encrypted image must be oscillated in a predefined direction, under a predefined law of motion. The formation of time-averaged fringes helps to interpret the secret image; the secret is leaked in a form of a pattern of developed time-averaged moiré fringes. In other words, optical methods (and the basic principles used to encrypt and decrypt the secret image) are completely different in our approach and methods described in Refs. [22,23].

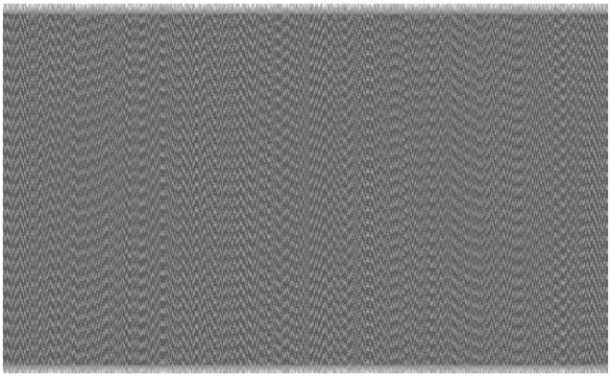

Fig. 14. The secret image cannot be leaked when oscillations are harmonic; the time-averaged image is shown at $s = \frac{r_1\lambda_1}{2\pi} = 0.6433$ mm.

Fig. 15. The secret image "cameraman".

As mentioned previously, our method cannot be directly compared to techniques used to encrypt a digital image in Refs. [22,23]. Nevertheless, it would be advantageous to compute formal parameters describing the quality of encryption. Correlation of pixels, entropy, PSNR and the histogram distribution can provide useful information on the pixel distribution in respect to the original image [23].

We use a cameraman black and white digital image (Fig. 15) to test the functionality of our method. So far, we have been encoding a secret image into near-optimal moiré gratings placed into vertical columns of pixels. Accordingly, oscillations used for the visual decoding of the secret had to be uni-directional oscillations along the vertical axis of the encoded image. Now we use a 15° inclined near-optimal moiré gratings to encode the image (Fig. 16). It should be noted that we do not use a pixel confusion–diffusion algorithm in the encoding process (what would damage the regular structure of the moiré grating carrying the secret visual information).

Correlation plots of pixels in the encoded image in the direction of the x-axis and the y-axis are presented in Figs. 17 and 18. As mentioned previously, we did not use any pixel shuffling or confusion–diffusion algorithms to encrypt the image. Anyway, the distribution of neighboring pixels in Figs. 17 and 18 show almost random nature of the distribution of pixels in the encoded image (a full square of dots would denote a completely random distribution of pixels).

Fig. 19 presents the computationally decoded image (15° inclined uni-directional zig-zag type oscillations were used to decrypt the

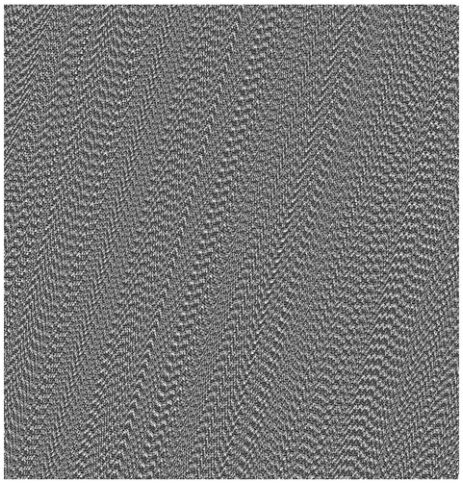

Fig. 16. The secret image encoded in an inclined near-optimal moiré grating.

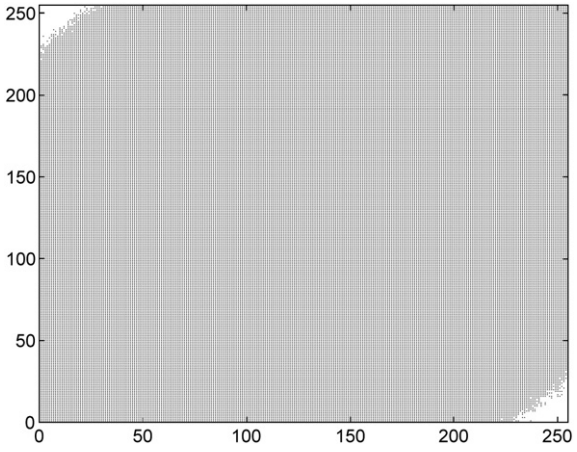

Fig. 17. The distribution of pixels in rows of the encoded image.

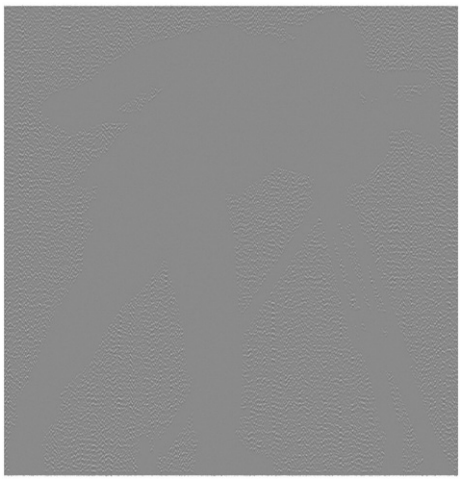

Fig. 19. Computationally decoded secret image.

secret image). We use the contrast enhancement algorithm [21] to reveal the pattern of time average fringes in Fig. 19 the resulting digital image is presented in Fig. 20. It can be noted that certain erosion of pixels can be observed at the boundary between the secret image and the background. That can be explained by the oscillatory nature of the decoding procedure.

We use the standard algorithm for the computation of the entropy of digital images [24] in order to assess the distribution of pixels in the encoded image. The entropy of the original image (Fig. 15) is 2.5399; the entropy of the encoded image (Fig. 16) is 7.7017; the entropy of the decoded image (Fig. 19) is 2.5049; and the entropy of Fig. 20 is 1.8128. The entropy of the encoded image is more than 3 times higher compared to the original image. That is a very good result (a higher entropy corresponds to a higher randomness) keeping in mind that we did not diffuse or shuffle pixels of the original image during the encryption. The entropy of the decoded image is lower than the entropy of the original image. It can be explained by the fact that the time-averaged moiré fringes do smooth local roughness of the original image [16]. A special contrast enhancement algorithm [21] makes the image even more uniform; thus the entropy of Fig. 20 is the lowest one.

PSNR [25] between the original image (Fig. 15) and the decoded image (Fig. 20) is 8.8142. This assessment is not very favorable to our technique; a better result could be achieved by the method described in Refs. [22,23]. Anyway, one must keep in mind that our technique is based on the formation on time-averaged moiré fringes — not double-exposure moiré fringes. The optical principle of the formation of moiré fringes is completely different. Thus a straightforward comparison between those two techniques is irrelevant. Our method works well with larger objects; smaller details are blurred due to the shorter moiré gratings which are used to encode the secret image. Inevitable oscillations around the state of the image's equilibrium cause optical blur at boundaries of the secret image. What is even more important, a whole number of periods of the moiré grating may not fit into a smaller component of the secret image. This is a definite drawback of the proposed technique. Anyway, our technique has a number of advantageous features. This is a single share method; no overlapping of any shares is required for the formation of the secret image. In this respect, a worse value of the PSNR assessment can be compensated by the added-value of the functionality of the proposed technique.

The histogram of the encoded image (Fig. 16) is shown in Fig. 21. Again, one should keep in mind that the pixel confusion–diffusion algorithm has not been used to encrypt the secret image; the regular structure of the moiré grating has been preserved in the encoded image. Nevertheless, the histogram of the encoded image is rather rich compared to a histogram of the original image which would contain two discreet lines only.

The sensitivity of the encryption method can be measured by computing entropies and PSNR of two different encryptions in respect to a little change in the system's parameters [23]. Computational experiments are repeated with Fig. 15 but the angle of inclination is set to 15.1°. The entropy of the encoded image then equals to 17.212. Though the change in the entropy (compared to the encoding at 15°)

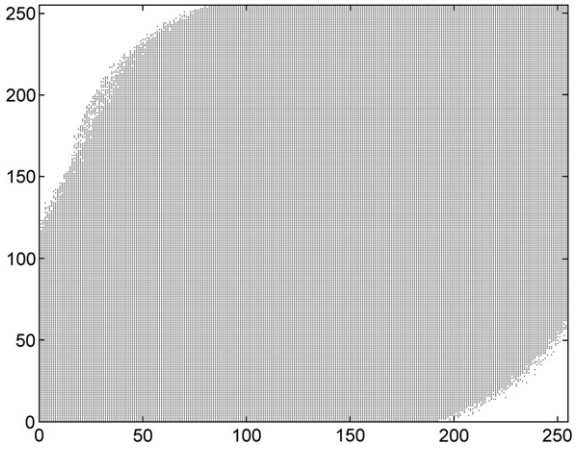

Fig. 18. The distribution of pixels in columns of the encoded image.

Fig. 20. Contrast enhanced pattern of time-averaged moiré fringes reveals the secret image.

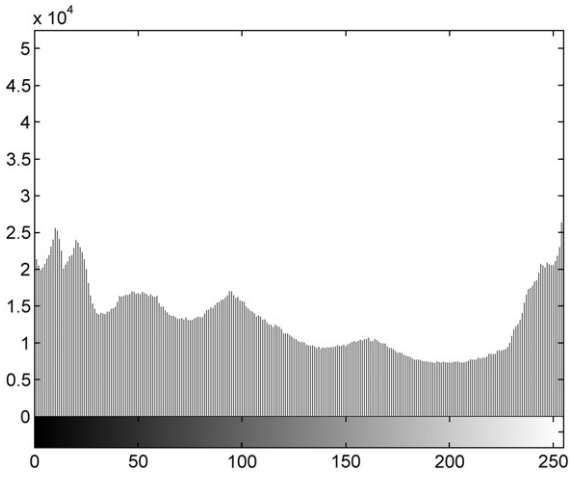

Fig. 21. The histogram of the encoded image.

is not high, the structure of the encoded image experiences a considerable alternation simply due to the different arrangement of the moiré grating. PSNR between the original image and the decoded image is almost the same (8.8025) and demonstrates the functionality of the visual decryption technique. Anyway, one must keep in mind that the proposed method is not a moiré hash function [16] and a small change in the initial data (the secret image) does not cause an avalanche effect in the encrypted image. As mentioned previously, the proposed technique works well when the size of the secret geometrical objects is few times greater that the length of one period (pitch) of the near optimal moiré grating. A small change in one of few pixels in the secret image would have no effect to the decoded image.

Time needed to encrypt a secret image can be measured using a specific computational platform. The decryption can be performed completely visually (without a computer) so the assessment of the computational decryption time is irrelevant (though the decryption time is comparable to the encryption time). The size of the digital image in Fig. 15 is 500×545 pixels; it takes 2.7 s to encrypt the secret image; the computational tool used in the experiments is AMD SempronTM Processor 3400+, 1.81 GHz, 512 MB RAM.

Comparisons between the proposed method and methods described in Refs. [22,23,26] can be continued considering different images which can be encrypted by appropriate techniques. Methods described in Refs. [22,23,26] can work with such traditional images like lenna, pepper or cameraman. Our method, on the contrary, can work only with black-and-white images. As a matter of fact our encoding technique is based on two grayscale levels (one level determines the secret image; another — the background). The decoding stage is based on the optical averaging in time while the encoded image is oscillated in a predetermined direction under a predetermined law of motion.

It is clear that every method has its advantages and drawbacks. Methods [22,23,26] perform the decoding by a simple overlapping (one operation by pixel) in the computational form and experimentally. As mentioned previously, our method (on the contrary) is a one-share method. That is really an important advantage of our method — one does not need to overlap any images in order to decode the secret. The encoded image needs to be oscillated instead — and time-averaged moiré fringes will release the secret. The main object of this paper is to propose a better grating than a stepped moiré grating (optical experiments with stepped gratings are presented in Ref. [14]). The drawback of this method is its ability to work with black-and-white images only. A special adaptation discussed in Ref. [14] could be used to encode a secret image containing three different grayscale levels. Nevertheless, the proposed technique cannot be used to encode a grayscale secret image.

8. Concluding remarks

We have extended the applicability of image hiding techniques based on time-averaged moiré fringes. The near-optimal moiré grating provides additional security of the encoded image, while the decoding procedure is kept completely visual. The main objective of this paper was to optimize the process of encoding, thus we did not focus on the aspects of the human perception of the vibrating image; only computational experiments have been performed.

The developed image hiding technique strictly speaking is not a visual cryptography method. We do not split the secret image into shares; all information on the secret is kept in one image. The interplay between moiré gratings, stochastic initial phase scrambling and phase regularization algorithms are used to encode the secret into the carrier image. It is important to note that a computer is not necessary to decode the image — a naked eye can interpret the embedded secret if the encoded image is oscillated in a predefined direction at predefined amplitude and according to a predefined time function. Simple physical experiments in Ref. [14] (with harmonic moiré gratings and harmonic oscillations of course) demonstrate the effectiveness of the proposed method.

Applicability of other time functions such as the “zig-zag” type function, peculiarities of the human perception, coupling this image hiding method with image sharing techniques are natural objectives of future research.

References

[1] M. Naor, A. Shamir, Lect. Notes Comput. Sci. 950 (1994) 1.
[2] G. Ateniese, C. Blundo, A.D. Santis, D.R. Stinson, Theor. Comput. Sc. 250 (2001) 143.
[3] C.C. Lin, W.H. Tsai, Pattern Recognit. Lett. 24 (2003) 349.
[4] D.S. Tsai, G. Horng, T.H. Chen, Y.T. Huang, Inform. Sci. 179 (2009) 3247.
[5] Y.F. Chen, Y.K. Chan, C.C. Huang, M.H. Tsai, Y.P. Chu, Inform. Sci. 177 (2007) 4696.
[6] D. Wang, L. Zhang, N. Ma, X. Li, Pattern Recognit. 40 (2007) 2776.
[7] D.C. Lou, H.K. Tso, J.L. Liu, Comput. Stand. Inter. 29 (2007) 125.
[8] T.H. Chen, J.C. Huang, J. Syst. Software 83 (2010) 861.
[9] A.S. Kobayashi, Handbook on Experimental Mechanics, 2nd ed SEM, Bethel, 1993.
[10] K. Patorski, M. Kujawinska, Handbook of the Moiré Fringe Technique, Elsevier, Amsterdam, 1993.
[11] Y. Desmedt, T. Van Le, 7th ACM Conf. on Computer and Communications Security, 2000, p. 116.
[12] G. Lebanon, A.M. Bruckstein, J. Opt Soc. Am. A 18 (2001) 1371.
[13] G. Lebanon, A.M. Bruckstein, Lect. Notes Comput. Sc. 2134 (2001) 185.
[14] M. Ragulskis, A. Aleksa, Opt. Commun. 282 (2009) 2752.
[15] M. Ragulskis, A. Aleksa, Z. Navickas, J. Opt. A Pure Appl. Opt. 11 (2009) 125411.
[16] M. Ragulskis, Z. Navickas, Discrete Cont. Dyn B. 8 (2007) 1007.
[17] G.N. Watson, A Treatise on the Theory of Bessel Functions, Cambridge University Press, Cambridge, 1995.
[18] J.H. Holland, Adaptation in Natural and Artificial Systems: An Introductory Analysis with Application to Biology, Control, and Artificial Intelligence, 2nd ed. The MIT Press, Cambridge, 1992.
[19] D. Whitley, Statistics Computing 4 (1994) 65.
[20] http://www.edc.ncl.ac.uk/highlight/rhjanuary2007g01.php.
[21] M. Ragulskis, A. Aleksa, R. Maskeliunas, Opt. Lasers Eng. 47 (2009) 768.
[22] J.A. Munoz-Rodriguez, R. Rodriguez-Vera, Opt. Commun. 236 (2004) 295.
[23] J.A. Munoz-Rodriguez, Imaging Science J. 58 (2010) 61.
[24] http://www.mathworks.com/help/toolbox/images/ref/entropy.html.
[25] http://en.wikipedia.org/wiki/Peak_signal-to-noise_ratio.
[26] J.A. Munoz-Rodriguez, Revista Mexicana de Fisica 52 (2006) 53.